IET Power Electronics

Research Article

IET Journals
The Institution of Engineering and Technology

Application of the harmonic control arrays technique to single-phase stand-alone inverters

ISSN 1755-4535
Received on 2nd September 2015
Revised on 27th December 2015
Accepted on 16th January 2016
doi: 10.1049/iet-pel.2015.0687
www.ietdl.org

Mohammad-Sadegh Karbasforooshan[1], Mohammad Monfared[1] ✉, Murat Dogruel[2]

[1]*Department of Electrical Engineering, Faculty of Engineering, Ferdowsi University of Mashhad, Mashhad, Iran*
[2]*Department of Electrical and Electronics Engineering, Faculty of Engineering, Marmara University, Istanbul, Turkey*
✉ *E-mail: m.monfared@um.ac.ir*

Abstract: This study proposes the adaption of the harmonic control array (HCA) technique to control a single-phase stand-alone inverter system. The HCA method is recently proposed as an efficient scheme to control the systems with periodic references or disturbances. The HCA appropriately adjusts the harmonic components of the control signal to obtain a zero steady-state error. Since the signals and parameters involved in this method are complex valued, a discrete time implementation is presented for applying the method through a digital platform. The design procedure of the controller parameters are also presented by details. To confirm the theoretical achievements, experimental results for the prototype system are presented in this study. The results demonstrate the effectiveness of the proposed control scheme.

1 Introduction

Stand-alone inverters are widely used in industrial applications to supply sensitive loads or provide electric energy for local loads. Hence, the main aim of a stand-alone inverter system is to provide a regulated ac voltage, with low total harmonic distortion (THD), in spite of load disturbances and variations, to maintain a high-quality electric power flow to critical/local loads [1–5].

The stand-alone inverter system thus requires tracking or rejection of periodic signals. Several control methods to deal with periodic signals have been presented in literature [6–27]. From these, the stationary reference frame proportional resonant (PR) regulator [6–12], the synchronous reference frame (SRF) controller [13–20] and the digital repetitive controller [21–27] have shown successful performance. Although, the PR controller has the advantages of simplicity, low computational burden and zero steady-state error, but the response to step changes suffers from the exponential decay. Moreover, high sensitivity to the frequency variations of periodic signals and probability of instability to the phase shift of measured signals are attributed as other major disadvantages of the PR controller [6–12]. The SRF control technique transforms the system variables to a rotating frame at the synchronous speed, where the ac quantities become dc. Therefore, the signal in the SRF can be regulated by a simple proportional integral (PI) controller with zero steady-state error. Among the limitations of the SRF techniques are the need for several reference frame transformations, which increases the memory requirements and calculation errors, the limited application to balanced systems, complexity of algorithm and etc. [13–20]. Repetitive control which is based on the internal model principle is a very useful method that can track or reject periodic signals. The Bode plot of the repetitive controller has infinite amplitudes at multiples of the fundamental frequency that can lead to instability. Although many solutions to solve this problem are presented yet, but this method suffers from other drawbacks, such as a slow transient response, sensitivity to model accuracy and last but not least the high memory requirements [21–27].

The harmonic control array (HCA) technique is recently proposed for controlling systems involving reference and/or disturbance signals with periodic nature [28]. The HCA method automatically constructs the compensating periodic control signal and guarantees a perfect periodic reference tracking and disturbance rejection. However according to the control design structure, for many systems, the stabilisation and tracking could be achieved in a few periods, therefore this suggests that HCA method could be also successful for slowly varying non-periodic disturbances as well. HCAs use the running Fourier series integral to achieve the harmonic components of the reference and control signals. Although other control techniques may also be used in implementing HCAs, an array of PI controllers is employed in the present paper. The HCA method is easily applicable and effective on periodic reference tracking or periodic harmonic distortion compensation. For instance, it can be used for the selective harmonic compensation which brings extra flexibility in different power electronic applications, such as stand-alone or grid connected inverters, active power filters (APFs), power factor correction (PFC) circuits, etc. Selective harmonic detection and compensation in APFs can be a practical application of the HCA technique and lead to quality improvement and THD reduction of the voltage or current waveforms [29–31]. In grid connected inverters, selective harmonic control effectively mitigate the harmonic currents of concern [32, 33]. The other application is PFC circuits. In these circuits, the proposed technique can be included in the internal current control loop to effectively suppress the specific current harmonics [34]. In this paper, only brief information is provided for HCAs. Details of description, comparisons with alternative methods and numerical examples can be found in [28].

In this paper, a discrete time implementation procedure for the HCA method is provided so that the required algorithms can be easily and effectively implemented on digital systems. The procedure is applied to a single-phase stand-alone inverter voltage control system. The paper is organised as follows. First, the model of a single-phase stand-alone inverter, with an output LC filter, is described in Section 2. Then, the basics of the HCA method and its discrete time implementation are summarised in Section 3. Then, the step-by-step tuning procedure of controller parameters is provided in Section 4. Experiments of the presented system are coming in Section 5. Finally, the conclusions are drawn in Section 6.

2 Inverter model

The power and control circuits of a single-phase voltage-source stand-alone inverter are shown in Fig. 1. According to this figure, the power circuit consists of a full-bridge inverter, a LC-type

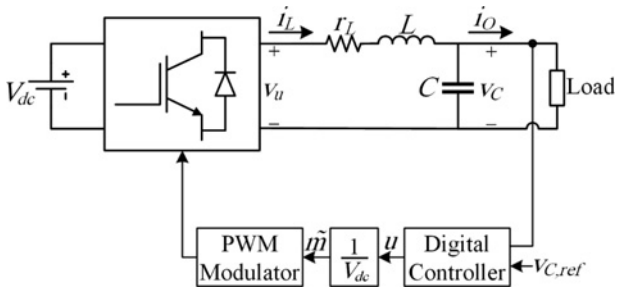

Fig. 1 *Voltage-source single-phase stand-alone inverter system: power and control stages*

Table 1 System parameters

Parameter	Symbol	Value
dc-link voltage	V_{dc}	250 V
nominal voltage	V_C	110 Vrms
nominal power	S	1 kVA
filter inductance	L	1 mH
filter capacitance	C	25 μF
ESR of the inductance	r_L	0.25 Ω
fundamental frequency	f	60 Hz
switching frequency	f_s	6 kHz

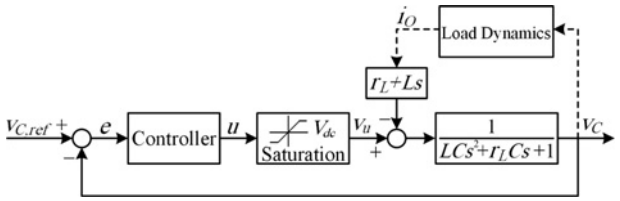

Fig. 2 *Block diagram of the control system*

smoothing filter and a local load. The parameters of the system under study are listed in Table 1. The state-space equations of the system can be readily written as

$$\frac{\mathrm{d}}{\mathrm{d}t}\begin{bmatrix} i_L \\ v_C \end{bmatrix} = \begin{bmatrix} -\frac{r_L}{L} & -\frac{1}{L} \\ \frac{1}{C} & 0 \end{bmatrix}\begin{bmatrix} i_L \\ v_C \end{bmatrix} + \begin{bmatrix} \frac{1}{L} & 0 \\ 0 & -\frac{1}{C} \end{bmatrix}\begin{bmatrix} v_u \\ i_o \end{bmatrix} \quad (1)$$

Then, the system transfer function is [3]

$$V_C(s) = \frac{1}{LCs^2 + r_L Cs + 1} V_u(s) - \frac{r_L + Ls}{LCs^2 + r_L Cs + 1} I_o(s) \quad (2)$$

Since the switching frequency of the PWM modulator is chosen to be much higher than the cut-off frequency of the LC low pass filter, by using the average switching model, one can approximately write

$$v_u \simeq \tilde{m} V_{\mathrm{dc}} = u \quad (3)$$

where m and u are the modulation index (in the range [0 1]) and the control input, respectively. Therefore, the corresponding block diagram of the system is shown in Fig. 2.

3 HCAs method

Fig. 3 shows a general feedback control system, with the HCA structure, where r is the reference input, u is the control signal and y is the system output.

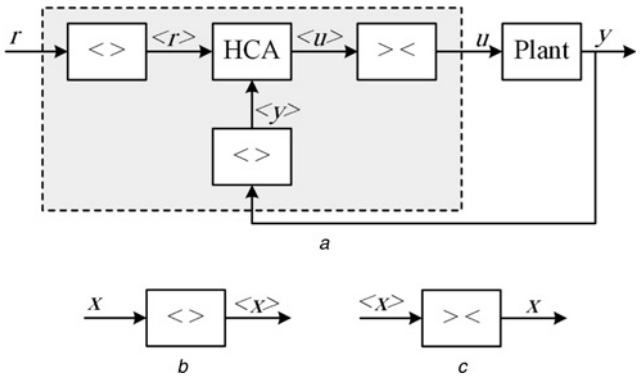

Fig. 3 *HCA block diagram*

a General structure
b Disperser
c Assembler

A *harmonic disperser* (Fig. 3*b*) extracts the time domain running harmonic components of the input signal as follows

$$\langle x\rangle_{\mathrm{h}}(t) = \frac{1}{T}\int_{t-T}^{t} x(\tau)\,\mathrm{e}^{-jh\omega\tau}\,\mathrm{d}\tau \quad (4)$$

where h represents the harmonic number, T and $\omega = 2\pi/T$ are the period and the angular frequency of the fundamental component of the reference signal, respectively.

For a digital implementation, the Fourier transform of (4) can be readily discretised with a predefined digital sampling rate. If the harmonic components of interest are from 0 to H, then the harmonic dispersion of $x(t)$ is shown as

$$\langle x\rangle = \begin{bmatrix} \langle x\rangle_0 \\ \langle x\rangle_1 \\ \vdots \\ \langle x\rangle_H \end{bmatrix} \quad (5)$$

Here, H is a design parameter reflecting the maximum harmonic order considered ($x(t)$ must not contain any major harmonic with an order higher than H). In practice, the right value for H can be chosen based on the application requirements and the calculation power of the real platform. By increasing H., more harmonics are controlled at the cost of more computational burden. To successfully accomplish all calculations within one sampling period, the upper limit for H may be compromised in some cases. However, with the increasing computational power of recent digital signal controllers and availability of efficient algorithms, the realisation of such operations with a high value for H are becoming possible for even very short sampling periods.

A *harmonic assembler* (Fig. 3*c*) reconstructs a time varying signal from its harmonic components as

$$x(t) = \langle x\rangle_0(t) + 2\mathrm{Re}\left\{\sum_{h=1}^{H}\langle x\rangle_h(t)\,\mathrm{e}^{jh\omega t}\right\} \quad (6)$$

The HCA block in Fig. 3*a* gives $\langle r\rangle$ and $\langle y\rangle$ as inputs and decides the control signal $\langle u\rangle$. In this work, the HCA block is realised by proportional-integral (PI) controllers. The corresponding block diagram of the HCA for our problem is simply shown in Fig. 4 and the harmonic dispersion of the control signal $\langle u\rangle$ is calculated as

$$\langle u\rangle = K_{\mathrm{P}}\langle e\rangle + K_I\int_{-\infty}^{t}\langle e\rangle\,\mathrm{d}t \quad (7)$$

where $e = v_{C,\mathrm{ref}} - v_C$ is the error signal. The integral term in (7) can be protected by an *anti-windup* algorithm. Moreover, the *magnitude* of

IET Power Electron., 2016, Vol. 9, Iss. 7, pp. 1445–1453

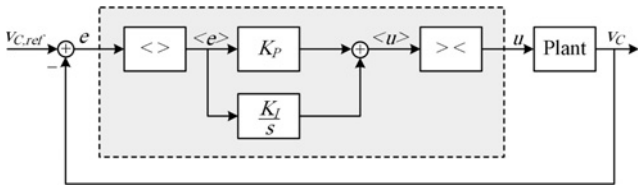

Fig. 4 *Harmonic PI control array*

the control signal can be saturated to prevent the operation of the converter in the overmodulation region.

As already seen, to use the HCA method, the implementation of the harmonic disperser (4), the HCA block (7) and the harmonic assembler (6) are necessary in the discrete form. To realise these, let us use a sampling period of T_s such that $N = T/T_s$ is an integer number. The ratio N/H, as representing the number of points in one sinusoidal period of the highest harmonic, should be as high as possible to get a satisfactory approximation in discrete domain.

The discrete time version of the harmonic disperser of (4) can then be obtained as

$$\begin{aligned}\langle x\rangle_{\mathrm{h}}[n] &= \frac{1}{N}\sum_{k=n-N+1}^{n} x[k]\,\mathrm{e}^{-\mathrm{j}h\omega kT_s} \\ &= \frac{1}{N}\sum_{k=n-N+1}^{n} x[k]\,\mathrm{e}^{-\mathrm{j}2\pi hk/N}\end{aligned} \tag{8}$$

where $x[k] = x(kT_s)$ and $\langle x\rangle_{\mathrm{h}}[n]$ approximately represents $\langle x\rangle_{\mathrm{h}}(nT_s)$. Note that the exponential term in (8) is a periodic function in time, that is

$$\mathrm{e}^{-\mathrm{j}2\pi hk/N} = \mathrm{e}^{-\mathrm{j}2\pi h(k+N)/N} \tag{9}$$

for each integer k, therefore, it is enough to calculate these terms for one period (for a total of N cases) only. After recording these values for $k = 0, 1, \ldots, N-1$, instead of recalculating each time, these values can be called from the memory. Another important calculation time saving can be achieved, noting that the sum in (8) is carried out for a limited period, and many common terms are present in the addition. To this end, (8) can alternatively be written as

$$\langle x\rangle_{\mathrm{h}}[n] = \langle x\rangle_{\mathrm{h}}[n-1] + \frac{1}{N}\left(x[n] - x[n-N]\right)\mathrm{e}^{-\mathrm{j}2\pi hn/N} \tag{10}$$

This last equation, requiring only one complex multiplication, greatly simplifies the calculation load of the harmonic disperser and suggests a feasible way to find the dispersion of the signal $x(t)$ (or $e(t)$) in the discrete time. This equation can be rewritten as

$$\langle x\rangle_{\mathrm{h}}[n] - z^{-1}\langle x\rangle_{\mathrm{h}}[n] = \frac{1}{N}\left(x[n] - z^{-N}x[n]\right)\mathrm{e}^{-\mathrm{j}2\pi hn/N} \tag{11}$$

The transfer function of the disperser in the z-domain is obtained as

$$G_{\mathrm{disperser}}(z) = \frac{\langle x\rangle_h[n]}{x[n]} = \frac{1}{N}\left(\frac{1-z^{-N}}{1-z^{-1}}\right)\mathrm{e}^{-\mathrm{j}2\pi hn/N} \tag{12}$$

The PI HCA block (7) can also be implemented in discrete time using

$$\langle u\rangle[n] = K_{\mathrm{P}}\langle e\rangle[n] + K_{\mathrm{I}}E[n] \tag{13}$$

where E represents the integral of $\langle e\rangle$ in discrete time and can be calculated as

$$E[n] = E[n-1] + T_s\langle e\rangle[n] \tag{14}$$

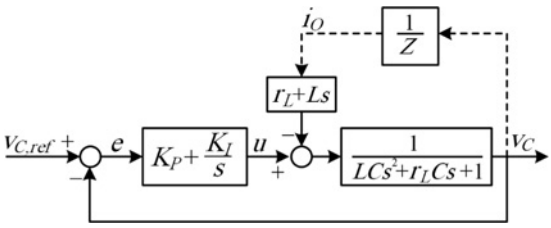

Fig. 5 *Simplified block diagram of the single-phase inverter control system*

To find the real control action u to be applied to the modulator, on the other hand, (6) can be transferred to the discrete domain as

$$u[n] = \langle u\rangle_0[n] + 2\mathrm{Re}\left\{\sum_{h=1}^{H}\langle u\rangle_h[n]\,\mathrm{e}^{\mathrm{j}2\pi hn/N}\right\} \tag{15}$$

4 Controller parameter design

The block diagram of the converter in presence of the HCA controller is shown in Fig. 4. It is possible to simplify this model by neglecting the assembler and disperser dynamics and modeling the load dynamics by an impedance Z. Then the controller parameters are designed based on the simplified model shown in Fig. 5.

Conventionally, a small resistor is connected in series with the filter capacitor to damp the high-frequency resonances from the switching harmonics, which its effect on the dynamics of the control system can be reasonably neglected.

It is observed that under light loads (Z tends to ∞), the phase margin (PM) and the closed loop stability of the system are decreased [13]. Therefore, the controller is designed and its parameters are tuned under the worst condition; that is, the no load. As a conservative assumption, this ensures that the system PM will never become smaller than the desired value for a wide range of operating conditions. The simplicity of the controller design is another benefit of neglecting the load dynamics. Under this condition, the plant transfer function simplifies to

$$G_{\mathrm{P}}(s) = \frac{v_C(s)}{u(s)} = \frac{1}{LCs^2 + r_LCs + 1} \tag{16}$$

and the loop gain is

$$\frac{v_C(s)}{e(s)} = \frac{K_{\mathrm{P}} + (K_{\mathrm{I}}/s)}{LCs^2 + r_LCs + 1} \tag{17}$$

Tuning the PI controller is essentially a tradeoff between the attainable control bandwidth and the loop stability [13]. The integral part of the PI controller provides a high gain at zero frequency and its effect around the loop cross-over frequency, and therefore the bandwidth frequency (ω_{b}), can be neglected, especially in the case of a large bandwidth. Hence, first it is assumed that $K_{\mathrm{I}} = 0$ and the transfer function of the closed loop system becomes

$$\left.\frac{v_C(s)}{v_{C,\mathrm{ref}}(s)}\right|_{K_I=0} = \frac{K_{\mathrm{P}}}{LCs^2 + r_LCs + K_{\mathrm{P}} + 1} \tag{18}$$

Considering −3 dB attenuation for (18) at the bandwidth frequency ω_{b} yields to

$$\frac{K_{\mathrm{P}}}{\sqrt{\left(K_{\mathrm{P}} + 1 - LC\omega_{\mathrm{b}}^2\right)^2 + \left(r_LC\omega_{\mathrm{b}}\right)^2}} = \sqrt{\frac{1}{2}} \tag{19}$$

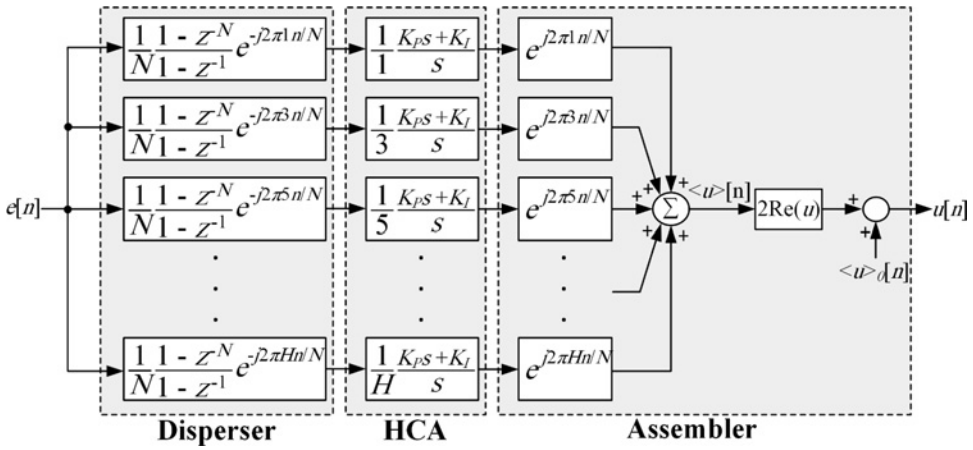

Fig. 6 *Overall structure of the HCA control system*

from which, the proportional gain K_P is calculated as

$$K_P = 1 - LC\omega_b^2 + \sqrt{2\left(LC\omega_b^2 - 1\right)^2 + \left(r_L C\omega_b\right)^2} \qquad (20)$$

The control bandwidth of the system in this application is a tradeoff between the transient response and the switching noise rejection capability, which in this paper is selected to be 900 Hz. With this selection, a high dynamic performance and at the same time a proper immunity of the control loop to switching noises is ensured. Substituting $\omega_b = 2\pi \times 900$ rad/s into (20) gives $K_P = 0.48$.

After calculating K_P, based on the selected bandwidth and the filter parameters, the proper value of K_I must be determined according to stability requirements. For this end, the simultaneous effect of K_I and K_P will be considered.

Assuming that the cross-over frequency of the loop gain (17) is close to the closed-loop bandwidth, ω_b, it is possible to examine the stability degree, in terms of the PM, from the loop gain (17). Accordingly, the phase of transfer function (17) at ω_b is set equal to PM-π. The result is shown in (21). To ensure the stable operation of the system, especially in presence of unmodelled dynamics, such as the delays associated to the assembler, disperser and PWM modulator, a PM in the range of 70°–100° is recommended. Evaluating (21) for PM = 85° and $K_P = 0.48$ (already determined), yields $K_I = 100.6$.

$$\tan(\mathrm{PM} - \pi) = \frac{\omega_b\left(\left(LK_I - r_L K_P\right)C\omega_b^2 - K_I\right)}{K_I^2 + \left(K_P\left(K_P + 1 - LC\omega_b^2\right) - r_L CK_I\right)\omega_b^2} \qquad (21)$$

The resulted K_P and K_I are the PI control parameters for the fundamental frequency component. In other words, these parameters are designed for the case $h = 1$. The control parameters for higher harmonics ($h = 3, 5, \ldots$) are obtained by dividing K_P and K_I by h. The overall structure of the HCA control system is shown in Fig. 6.

5 Performance evaluation

In this section, the simulation and experimental results of the prototype system, with the same parameters of Table 1, are presented. The nominal frequency is 60 Hz and the switching frequency is selected such that f_s/f becomes an integer ($N = 100$).

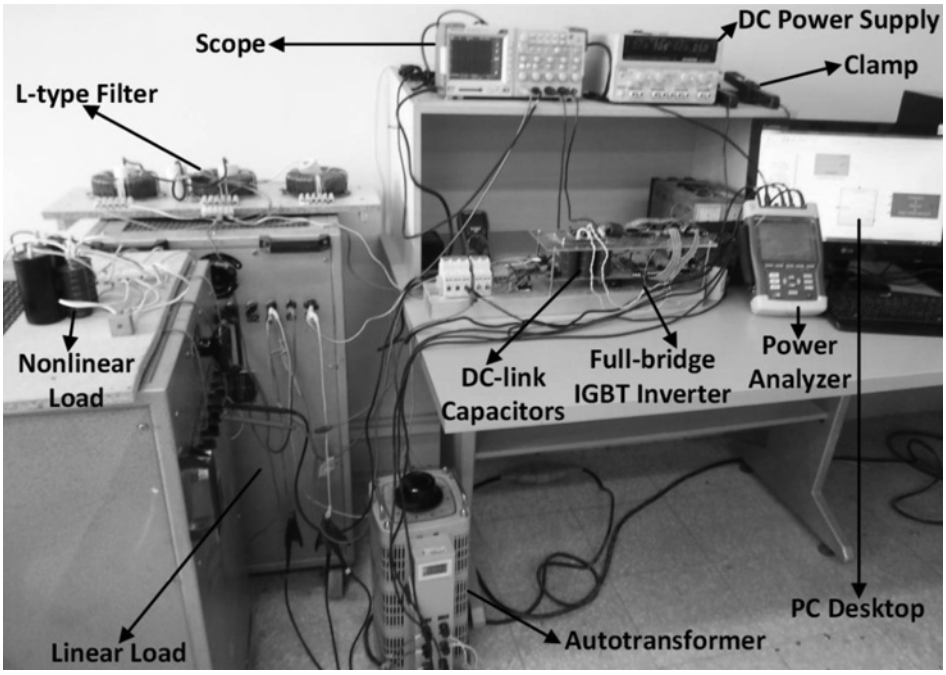

Fig. 7 *Experimental setup*

IET Power Electron., 2016, Vol. 9, Iss. 7, pp. 1445–1453

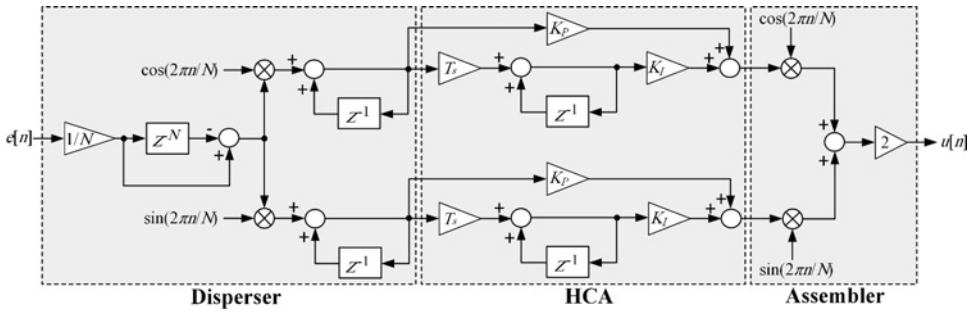

Fig. 8 *Digital implementation of the proposed control method*

The simulations are conducted in MATLAB/Simulink environment. The experimental setup is shown in Fig. 7, which consists of dc-link capacitors fed from a diode rectifier circuit, a full-bridge IGBT inverter, a LC-type output filter and measurement devices. The control algorithm is implemented on a TMS320F28335 digital signal controller from TI. The digital implementation of the proposed control algorithm is shown in Fig. 8. In this figure, the disperser, assembler and the HCA blocks are separately implemented in a digital form.

The simulated and experimental steady-state waveforms and the output voltage harmonic spectrum of the converter system when the nominal resistive load is connected to the output are shown in Figs. 9*a* and 10*a*, respectively. The results of simulations and experiments are in good accordance, where the output voltage waveform is highly sinusoidal with THD = 0.56 and 1.5% for simulation and experiment, respectively. In this test, only the fundamental harmonic component is considered for compensation; that is, $H = 1$.

In the second study, the simulation and experimental results for a capacitive (lightly damped) load are reported in Figs. 9*b* and 10*b*, respectively. While the load power factor is <0.7, the output voltage THD remains below 0.6% in simulation and below 1.6% in experimental test. In the final steady-state performance verification, a highly distorted and non-linear load, according to the IEC 62040-3 standard (Annex E) requirements [35], is connected to the output of the single-phase inverter. This load is a diode rectifier bridge feeding a parallel RC load (20 Ω || 6.8 mF) through a small resistor (4 Ω). The results, when only the fundamental component compensation is included in the control loop ($H = 1$), are shown in Figs. 11*a* and 12*a*. The THD of the output voltage in simulation is 3.39% and in experimental test is 4.2% and the third and fifth harmonics of the output voltage have considerable magnitudes.

In the next experiment, the third and fifth harmonics compensation are also added to the control algorithm ($H = 5$) and the output results for the same loading condition are shown in Figs. 11*b* and 12*b*.

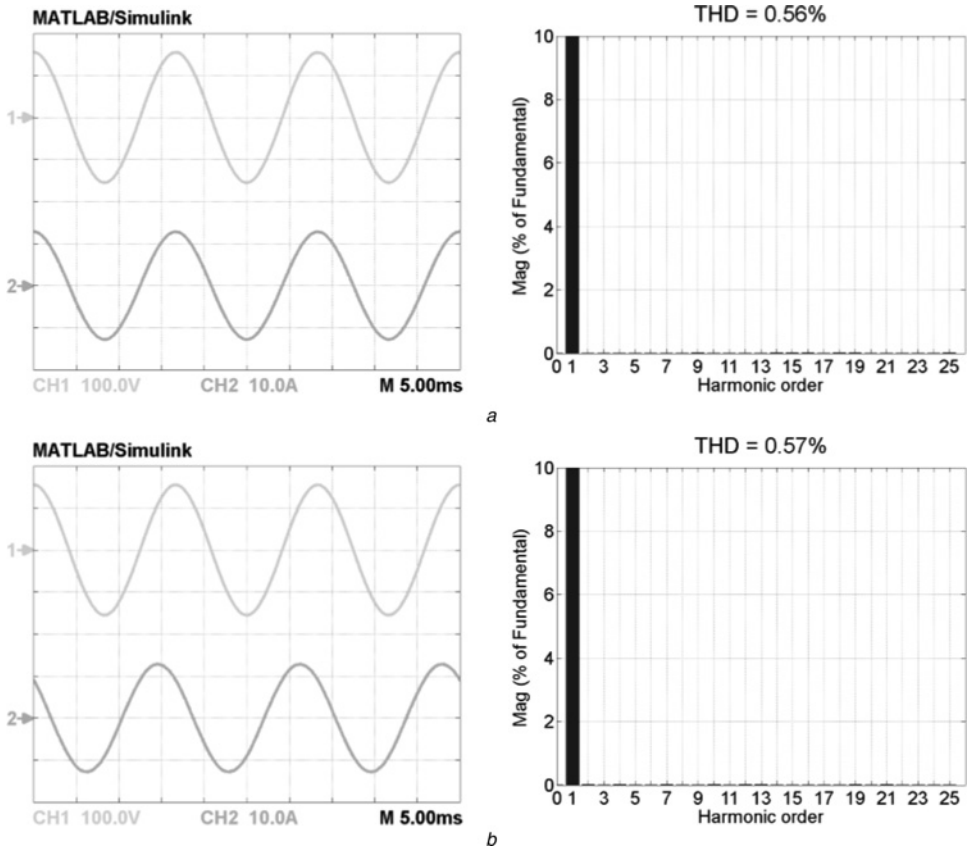

Fig. 9 *Simulated steady-state performance under*

a Nominal resistive load
b RC load: CH1: output voltage (100 V/div), CH2: load current (10 A/div)

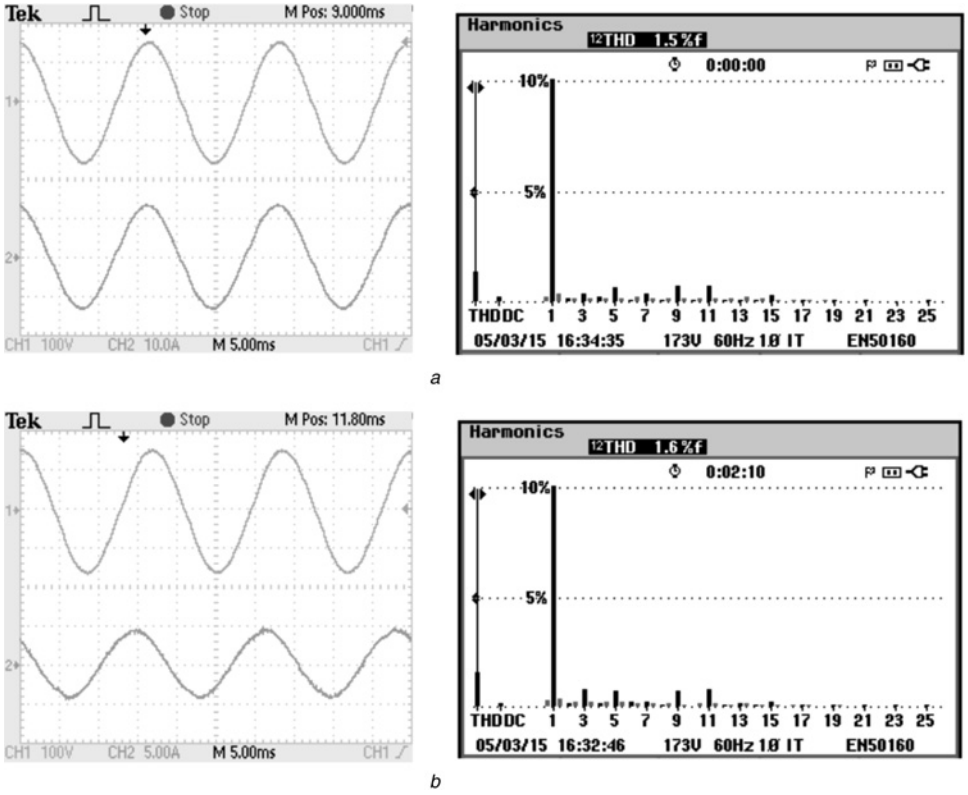

Fig. 10 *Experimental steady-state performance under*

a Nominal resistive load
b RC load: CH1: output voltage (100 V/div), CH2: load current (10 A/div)

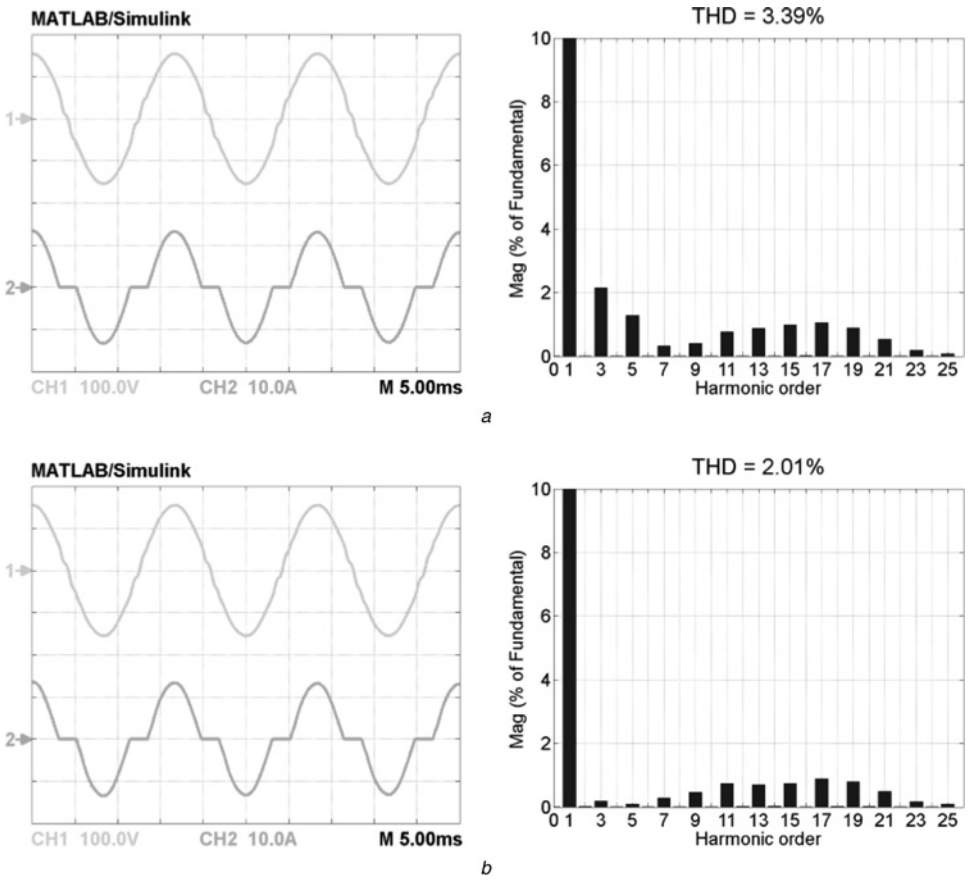

Fig. 11 *Simulated steady-state performance and output voltage harmonic spectrum under highly non-linear load, including*

a Only the fundamental component compensation
b Fundamental and the third and fifth harmonics compensation: CH1: output voltage (100 V/div), CH2: load current (10 A/div)

IET Power Electron., 2016, Vol. 9, Iss. 7, pp. 1445–1453

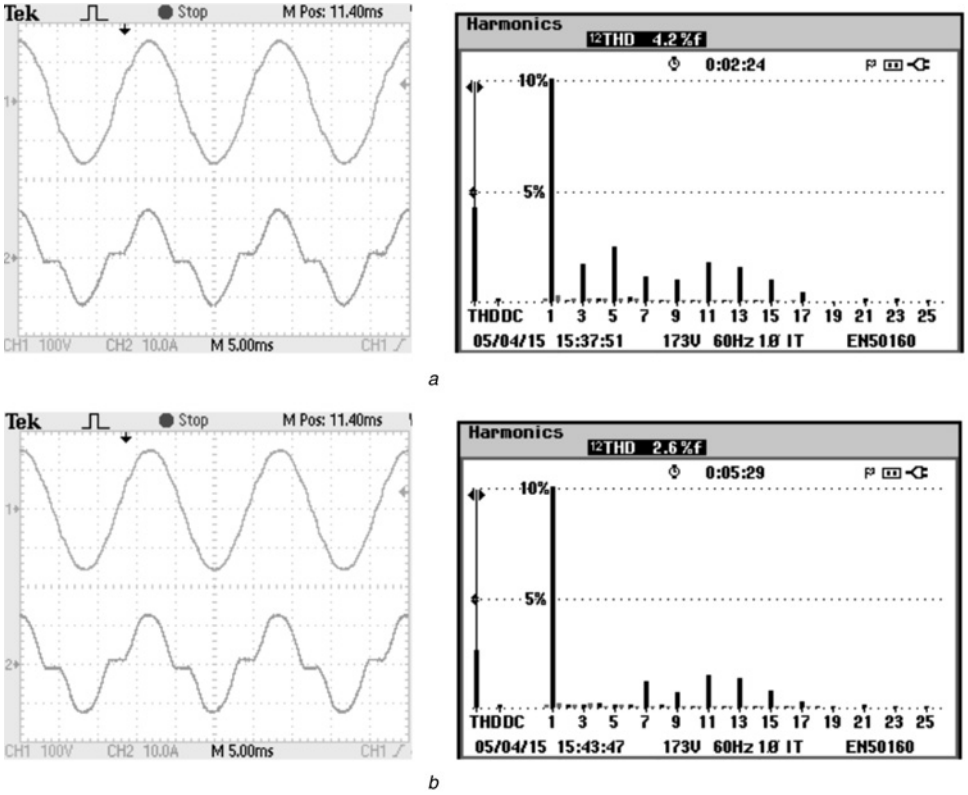

Fig. 12 *Experimental steady-state performance and output voltage harmonic spectrum under highly non-linear load, including*

a Only the fundamental component compensation

b Fundamental and the third and fifth harmonics compensation: CH1: output voltage (100 V/div), CH2: load current (10 A/div)

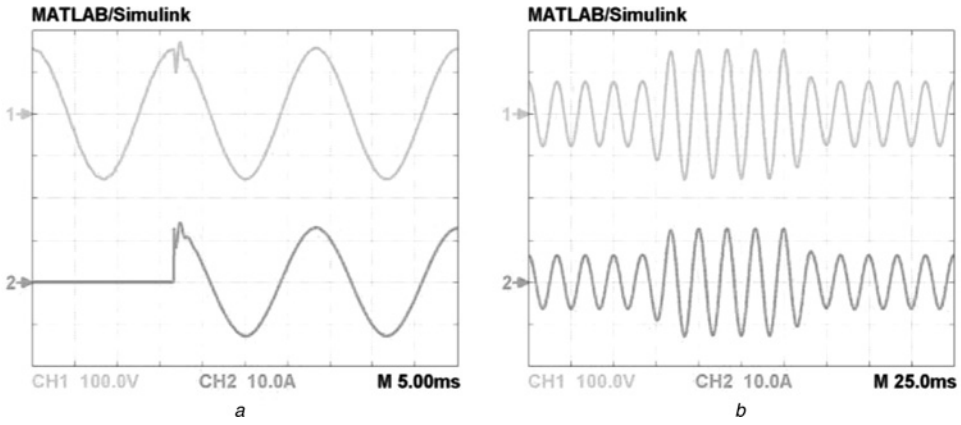

Fig. 13 *Simulated transient performance in response to*

a No-load to nominal resistive load step change

b +50% followed by −50% step change of reference voltage amplitude: CH1: output voltage (100 V/div), CH2: load current (10 A/div)

Obviously, the added harmonic compensators can efficiently mitigate the third and fifth harmonics from the output voltage. Then, the output voltage THD is improved in simulation and experiment to 2.01 and 2.6%, respectively, which is far below the standard limit of 8% [35]. However, it is possible to attenuate more harmonics of concern, according to the application requirements, by adding extra HCAs to the controller, at the price of more computation burden. Finally, the transient performance of the system was investigated, with only the fundamental compensation, and the results are depicted in Figs. 13 and 14. Evidently the simulations and experiments match well. In Figs. 13*a* and 14*a*, the transient performance in response to a load step change from no-load to nominal resistive load is shown. The output voltage experiences a small dip at the moment of load connection, which occurs around the voltage peak, and recovers in <2 ms. Figs. 13*b* and 14*b* show the transient performance of the system in response to a step jump followed by a step fall of the reference voltage magnitude under the nominal resistive load. A slow oscillation, with a very small overshoot/undershoot, can be recognised in the voltage waveform envelope, which safely dies in less than two cycles.

As already mentioned, the simulation and experimental results are in good agreement. However, the simulation and test results may differ in some details due to different non-idealities in the practical implementation. However, if this level of accuracy is not acceptable for some very especial simulation studies, more practical details such as the DC voltage ripples, sensor circuit non-idealities, switching rise/fall times, dead-time distortions,

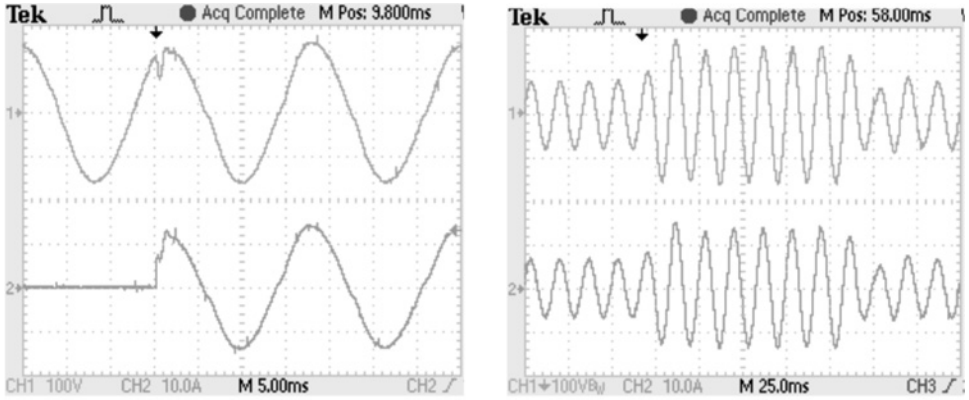

a *b*

Fig. 14 *Experimental transient performance in response to*

a No-load to nominal resistive load step change
b +50% followed by −50% step change of reference voltage amplitude: CH1: output voltage (100 V/div), CH2: load current (10 A/div)

non-linear characteristic of the filter inductor, circuit parasitic elements, etc. should be included in the simulation model.

6 Conclusion

This paper proposes the use of HCA method for the single-phase stand-alone inverters. The proposed control method ensures zero steady-state error at the fundamental frequency and other harmonics of interest. The main advantages of the HCA technique for the inverter applications are: possibility to compensate the harmonics and periodic disturbances in a selective way, which brings extra flexibility in different power electronic applications, such as stand-alone or grid connected inverters, APFs, PFC circuits, etc., simple concept and structure, simple digital implementation, precise tracking of AC signals and flexibility to employ any desired controllers in the HCA blocks, according to the application requirements. However, relatively slow dynamic response and the increasing computation burden by increasing the number of HCA blocks are the limitations of the proposed technique. The discrete time implementation of the HCA method along with a systematic procedure to design the control parameters are reported in this paper. The performance of the proposed scheme is confirmed with different experiments. The results indicate the effectiveness and excellent steady-state and transient performance of this method to control the single-phase stand-alone inverter.

7 References

1 Razi, R., Monfared, M.: 'Simple control scheme for single-phase uninterruptible power supply inverters with Kalman filter-based estimation of the output voltage', *IET Power Electron.*, 2015, **8**, (9), pp. 1817–1824
2 Lidozzi, A., Lo Calzo, G., Solero, L., *et al.*: 'Integral-resonant control for stand-alone voltage source inverters', *IET Power Electron.*, 2014, **7**, (2), pp. 271–278
3 Monfared, M.: 'A simplified control strategy for single-phase UPS inverters', *Bull. Polish Acad. Sci. Tech. Sci.*, 2014, **62**, (2), pp. 367–373
4 Wai, R.-J., Lin, C.-Y., Huang, H.-N., *et al.*: 'Design of backstepping control for high-performance inverter with stand-alone and grid-connected power-supply modes', *IET Power Electron.*, 2013, **6**, (4), pp. 752–762
5 Hasanzadeh, A., Edrington, C.S., Mokhtari, H., *et al.*: 'Multi-loop linear resonant voltage source inverter controller design for distorted loads using the linear quadratic regulator method', *IET Power Electron.*, 2012, **5**, (6), pp. 841–851
6 Gholami-Khesht, H., Monfared, M., Golestan, S.: 'Low computational burden grid voltage estimation for grid connected voltage source converter-based power applications', *IET Power Electron.*, 2015, **8**, (5), pp. 656–664
7 Hasanzadeh, A., Onar, O.C., Mokhtari, H., *et al.*: 'A proportional-resonant controller-based wireless control strategy with a reduced number of sensors for parallel-operated UPSs', *IEEE Trans. Power Deliv.*, 2010, **25**, (1), pp. 468–478
8 Herman, L., Papic, I., Blazic, B.: 'A proportional-resonant current controller for selective harmonic compensation in a hybrid active power filter', *IEEE Trans. Power Deliv.*, 2014, **29**, (5), pp. 2055–2065
9 Xia, C., Wang, Z., Shi, T., *et al.*: 'An improved control strategy of triple line-voltage cascaded voltage source converter based on proportional–resonant controller', *IEEE Trans. Ind. Electron.*, 2013, **60**, (7), pp. 2894–2908
10 Gholami-Khesht, H., Monfared, M.: 'Novel grid voltage estimation by means of the Newton–Raphson optimisation for three-phase grid connected voltage source converters', *IET Power Electron.*, 2014, **7**, (12), pp. 2945–2953
11 Teodorescu, R., Blaabjerg, F., Liserre, M., *et al.*: 'Proportional-resonant controllers and filters for grid-connected voltage-source converters', *IEE Proc. – Electr. Power Appl.*, 2006, **153**, (5), pp. 750–762
12 Vidal, A., Freijedo, F.D., Yepes, A.G., *et al.*: 'Assessment and optimization of the transient response of proportional-resonant current controllers for distributed power generation systems', *IEEE Trans. Ind. Electron.*, 2013, **60**, (4), pp. 1367–1383
13 Monfared, M., Golestan, S., Guerrero, J.M.: 'Analysis, design, and experimental verification of a synchronous reference frame voltage control for single-phase inverters', *IEEE Trans. Ind. Electron.*, 2014, **61**, (1), pp. 258–269
14 Mattavelli, P.: 'Synchronous-frame harmonic control for high-performance AC power supplies', *IEEE Trans. Ind. Appl.*, 2001, **37**, (3), pp. 864–872
15 Espi Huerta, J.M., Castello-Moreno, J., Fischer, J.R., *et al.*: 'A synchronous reference frame robust predictive current control for three-phase grid-connected inverters', *IEEE Trans. Ind. Electron.*, 2010, **57**, (3), pp. 954–962
16 Sha, D., Wu, D., Liao, X.: 'Analysis of a hybrid controlled three-phase grid-connected inverter with harmonics compensation in synchronous reference frame', *IET Power Electron.*, 2011, **4**, (7), pp. 743–751
17 Liu, X., Deng, Y., Liu, Q., *et al.*: 'Voltage unbalance and harmonics compensation for islanded microgrid inverters', *IET Power Electron.*, 2014, **7**, (5), pp. 1055–1063
18 Suul, J.A., Ljokelsoy, K., Midtsund, T., *et al.*: 'Synchronous reference frame hysteresis current control for grid converter applications', *IEEE Trans. Ind. Appl.*, 2011, **47**, (5), pp. 2183–2194
19 Sanatkar-Chayjani, M., Monfared, M.: 'Simple digital current control strategy for single-phase grid-connected converters', *IET Power Electron.*, 2015, **8**, (2), pp. 245–254
20 Zou, C., Liu, B., Duan, S., *et al.*: 'Stationary frame equivalent model of proportional-integral controller in dq synchronous frame', *IEEE Trans. Power Electron.*, 2014, **29**, (9), pp. 4461–4465
21 Lu, W., Zhou, K., Wang, D., *et al.*: 'A generic digital nk ± m-order harmonic repetitive control scheme for PWM converters', *IEEE Trans. Ind. Electron.*, 2014, **61**, (3), pp. 1516–1527
22 Chen, D., Zhang, J., Qian, Z.: 'Research on fast transient and 6n ± 1 harmonics suppressing repetitive control scheme for three-phase grid-connected inverters', *IET Power Electron.*, 2013, **6**, (3), pp. 601–610
23 Lu, W., Zhou, K., Wang, D., *et al.*: 'A general parallel structure repetitive control scheme for multiphase DC–AC PWM converters', *IEEE Trans. Power Electron.*, 2013, **28**, (8), pp. 3980–3987
24 Zhou, K., Wang, D., Zhang, B., *et al.*: 'Plug-in dual-mode-structure repetitive controller for CVCF PWM inverters', *IEEE Trans. Ind. Electron.*, 2009, **56**, (3), pp. 784–791
25 Ye, Y., Zhou, K., Zhang, B., *et al.*: 'High-performance repetitive control of PWM DC-AC converters with real-time phase-lead FIR filter', *IEEE Trans. Circuits Syst. II Express Briefs*, 2006, **53**, (8), pp. 768–772
26 Cheng, M., Zou, Z., Wang, Z., *et al.*: 'Fractional-order repetitive control of programmable AC power sources', *IET Power Electron.*, 2014, **7**, (2), pp. 431–438
27 de Almeida, P.M., Barbosa, P.G., Ribeiro, P.F., *et al.*: 'Repetitive controller for improving grid-connected photovoltaic systems', *IET Power Electron.*, 2014, **7**, (6), pp. 1466–1474
28 Dogruel, M., Çelik, H.H.: 'Harmonic control arrays method with a real time application to periodic position control', *IEEE Trans. Control Syst. Technol.*, 2011, **19**, (3), pp. 521–530
29 Lascu, C., Asiminoaei, L., Boldea, I., *et al.*: 'High performance current controller for selective harmonic compensation in active power filters', *IEEE Trans. Power Electron.*, 2007, **22**, (5), pp. 1826–1835

30 Miret, J., Castilla, M., Matas, J., *et al*.: 'Selective harmonic-compensation control for single-phase active power filter with high harmonic rejection', *IEEE Trans. Ind. Electron.*, 2009, **56**, (8), pp. 3117–3127
31 Mattavelli, P.: 'A closed-loop selective harmonic compensation for active filters', *IEEE Trans. Ind. Appl.*, 2001, **37**, (1), pp. 81–89
32 Yang, Y., Zhou, K., Wang, H., *et al*.: 'Frequency adaptive selective harmonic control for grid-connected inverters', *IEEE Trans. Power Electron.*, 2014, **30**, (7), pp. 3912–3924
33 Zhou, K., Yang, Y., Blaabjerg, F., *et al*.: 'Optimal selective harmonic control for power harmonic mitigation', *IEEE Trans. Ind. Electron.*, 2014, **62**, (2), pp. 1220–1230
34 Liu, B., Wu, J.J., Li, J., *et al*.: 'A novel PFC controller and selective harmonics suppression', *Int. J. Electr. Power Energy Syst.*, 2013, **44**, (1), pp. 680–687
35 IEC 62040-3: 'Uninterruptible power systems (UPS) – Part 3: Method of specifying the performance and test requirements'. 2011